

Bertrix (Wallonia, Belgium) Geophysical survey summary

DATE: December 2020



SUBJECT: ...

report
 information
 consideration
 decision

To: ...
 From: University of Liège & British Geological Survey

Index

Bertrix.....	3
Summary of the study area	3
Summary of available ground truth data	3
Geophysical investigations.....	4
Targeted sampling.....	17
Correlation analysis	18
Resource Distribution Model	21
Conclusion.....	23
References.....	25
Contact.....	26

Bertrix

Summary of the study area

Site history

The landfill of Bertrix (*Figure 1*) is located in the province of Luxembourg (Belgium). It was set up in a former quarry whose extent is unknown. Landfilling activities started in the 1970s with the deposit of Municipal Solid Waste (MSW). Nowadays, only the southern part of the landfill is still operational and receives inert waste. The surface area of the site is about 53 000 m² (see red polygon in *Figure 1*). As part of the RAWFILL project, the zone investigated by geophysical methods is located to the north of the site where, according to available information, the MSW were deposited. The area covered by geophysics is 11 300 m². The geophysical survey was conducted from 9 to 12 June 2020 and was prepared in close coordination with Idelux which manages the site.

Summary of available ground truth data

The information available on the site is very incomplete. No intrusive campaign has been carried out so that the available data on the composition of the waste, its location and thickness are very uncertain. In addition, no aerial photographs of the site were taken during the burial period of MSW, which makes it impossible to establish its precise location.

As the landfill was installed over a former quarry, it is likely that the waste directly lies on the bedrock. The latter is composed of siliceous shales, phyllades, quartzophyllades and stratoid sandstone of the Mirwart formation (formerly known as "Grès d'Anor et de Bastogne"). A topsoil layer of at least 1 m covers the entire area studied.

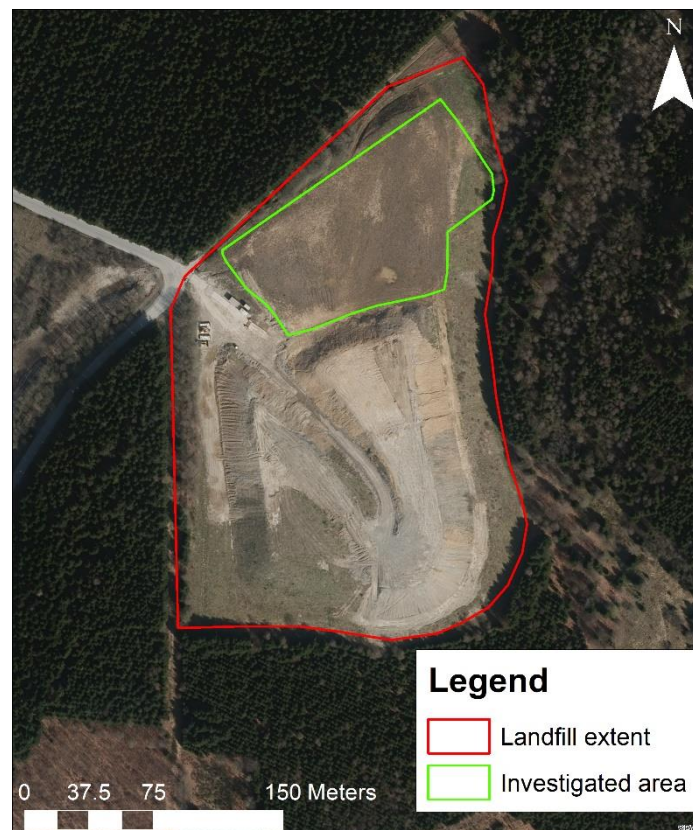


Figure 1: Overview of the Bertrix landfill (red polygon). The zone investigated in RAWFILL is the green polygon.

Geophysical investigations

Geophysical methods and coverage

The geophysical measurements in Bertrix involved Electromagnetics (EM, in-phase and out-of-phase at 3 different depths) to map the lateral extent and detect compositional changes within the waste. Electrical Resistivity Tomography (ERT), Induced Polarization (IP), Seismic Refraction Tomography (SRT), Multichannel Analysis of Surface Waves (MASW) and Horizontal to Vertical Spectral Ratio of Noise (HVSRN) were applied on several profiles crossing the landfill. These methods are expected to provide more detailed information about vertical extent and compositional changes. Illustrations of the geophysical setup is provided in *Figure 71*.

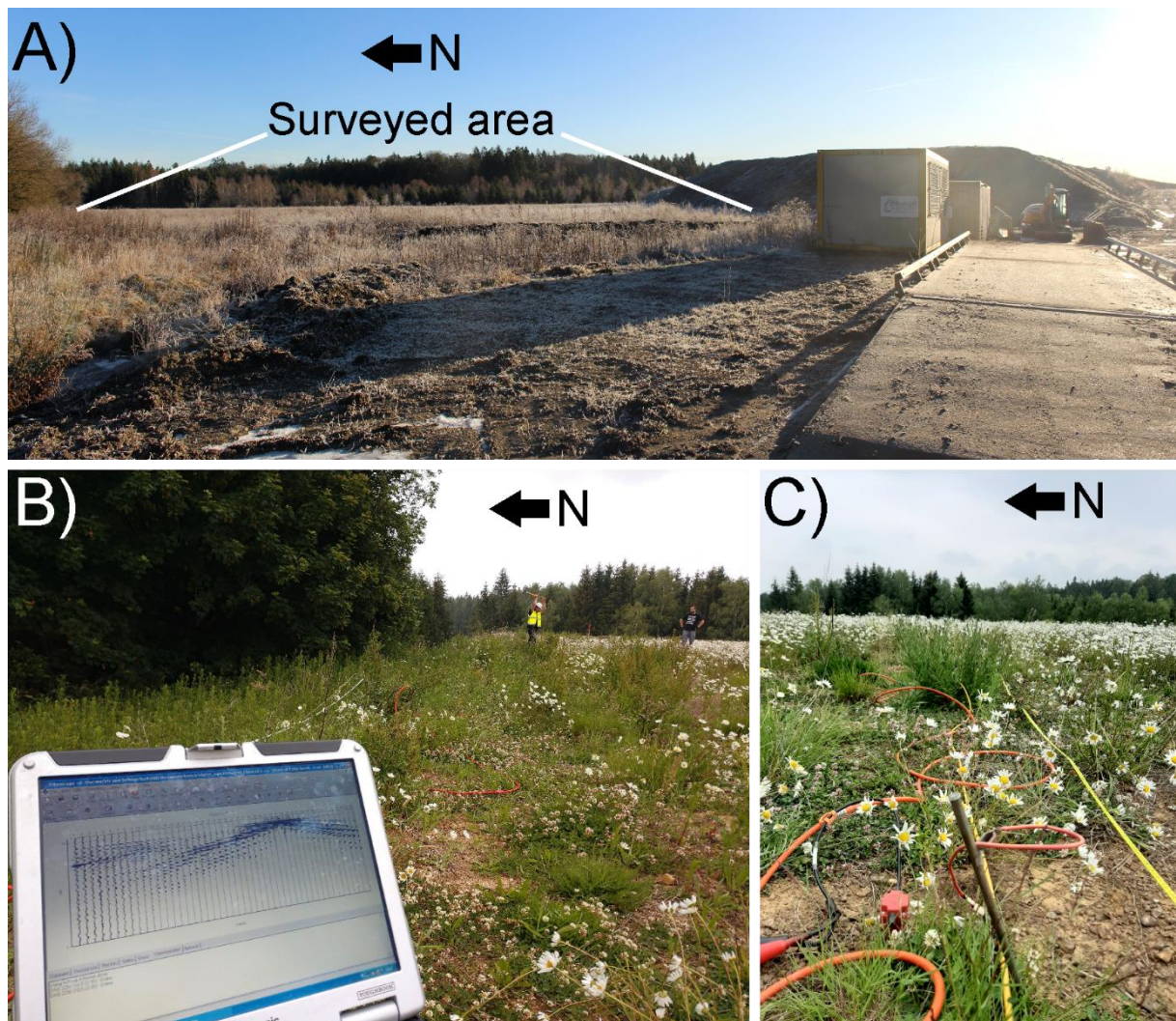


Figure 2: General view of the site (A), seismic acquisition (B) and ERT/IP setup (C)

In the following, the measurement parameters and spatial coverage of each method are described in more detail.

EM data were acquired using a Mini-explorer from GF Instruments. The Mini-explorer allows exploring simultaneously electrical properties at 0.5 m, 1 m and 1.8 m depths. Both quadrature (related to apparent conductivity) and in-phase (related to apparent magnetic susceptibility) components were recorded. In addition, a GPS sensor (without RTK correction) was connected to the system for positioning. Several parallel lines with a 2 m spacing were acquired in the area of interest. Data were also collected in the vicinity of the landfill for comparison purposes (*Figure 72*).

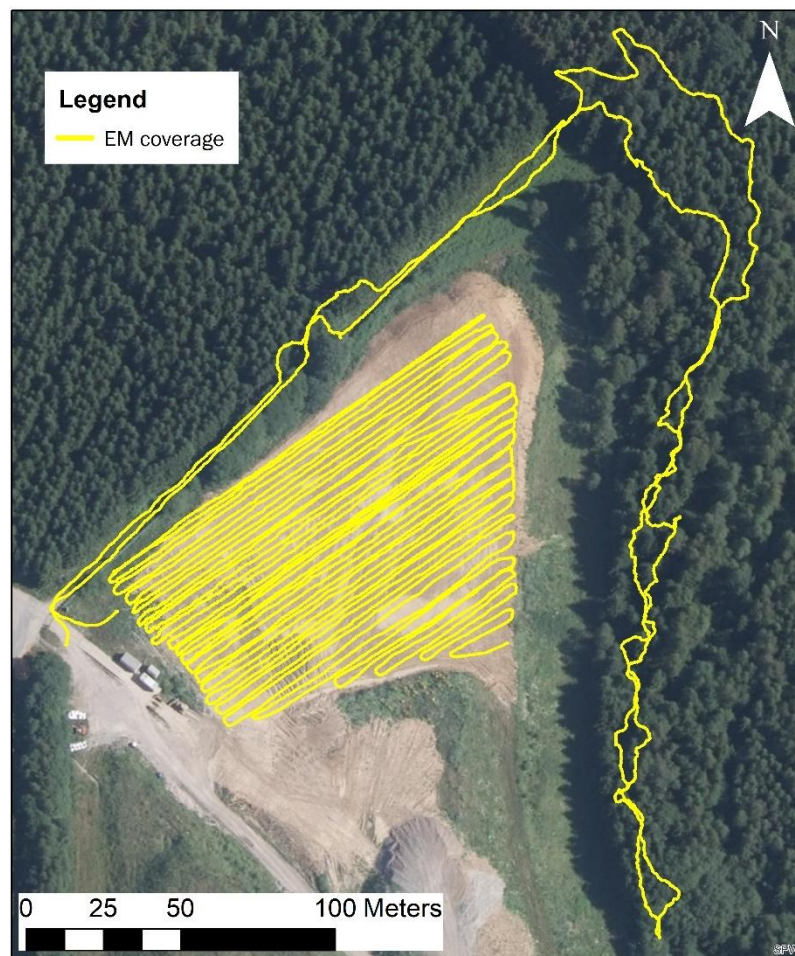


Figure 3: Coverage of the EM acquisition in the investigated area and surroundings of the landfill.

ERT and IP data were acquired with an ABEM Terrameter LS system. To derive a 3D resistivity/IP model, 13 parallel profiles were deployed (*Figure 73*). Each profile contained 32 stainless steel electrodes spaced by 5 m. The inter-profile spacing was set to 5 m. For the data acquisition, a gradient array with a 's' factor equals to 7 was used (Dahlin and Zhou, 2006). Measurements were not only carried out inline but also crossline. Electrical current injection was setup to 2 s (delay of 0.8 s and acquisition of 1.2 s) and the voltage decay was measured during 1.86 s after the current was switched off. Measurements were repeated twice to estimate the repetition error. A sample of reciprocal measurements was also collected for each profile to assess the quality of data.

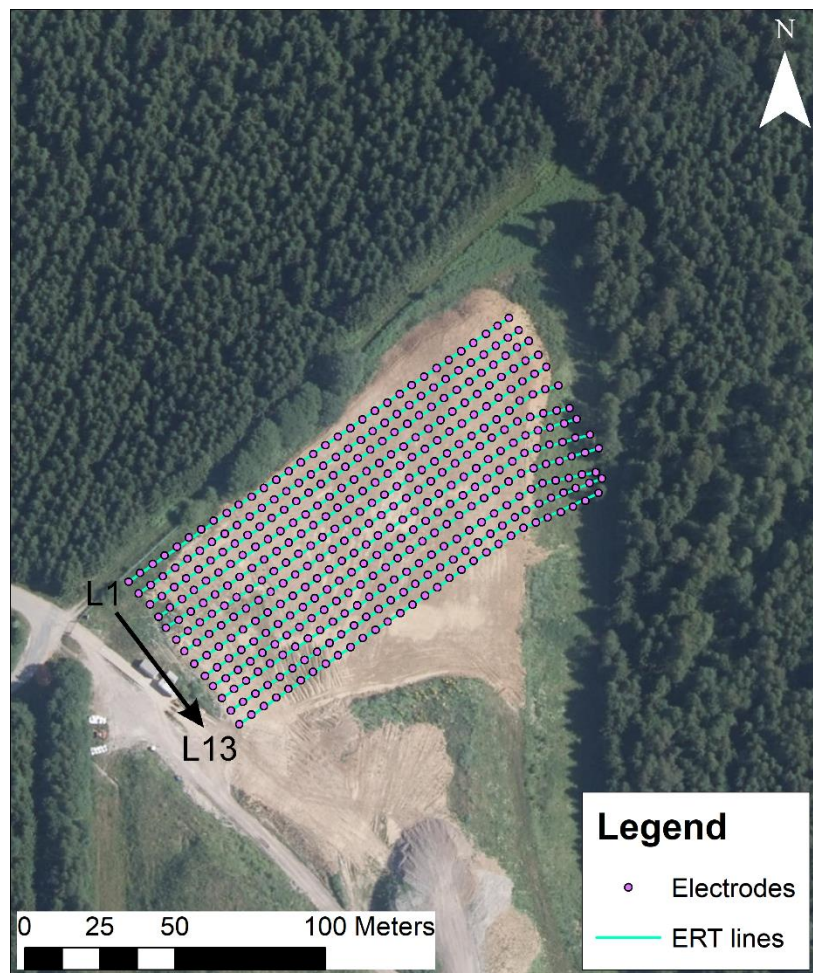


Figure 4: Coverage of the 3D ERT/IP acquisition.

Five MASW profiles were deployed in the location of some ERT/IP profiles (*Figure 74*). The data were acquired using a DAQlink 4 system and a fixed receiver array of 48 vertical geophones (4.5 Hz natural frequency) at 2.5 m intervals. A 5 kg sledgehammer was used as a source together with a ground-coupled nylon plate. The receiver array was kept fixed and the source was moved every four geophones (10 m) from off one extreme of the spread. In order to increase the signal to noise ratio, a total of 10 shots were stacked at each shot location. The SRT data were acquired using the same setup. For the HVSRRN acquisition, a seismometer LE-3Dlite MkIII (Lennartz) of 3 components and a low cut-off frequency of 1 Hz was used. The ambient noise was recorded at 18 locations across the site (8 points along the first MASW profile, 8 points along the second MASW profile and 2 points along the third MASW/SRT profile (see *Figure 74*). The HVSRRN stations were deployed with a spacing of 20 m and the recording time at each point was set to 25 minutes.

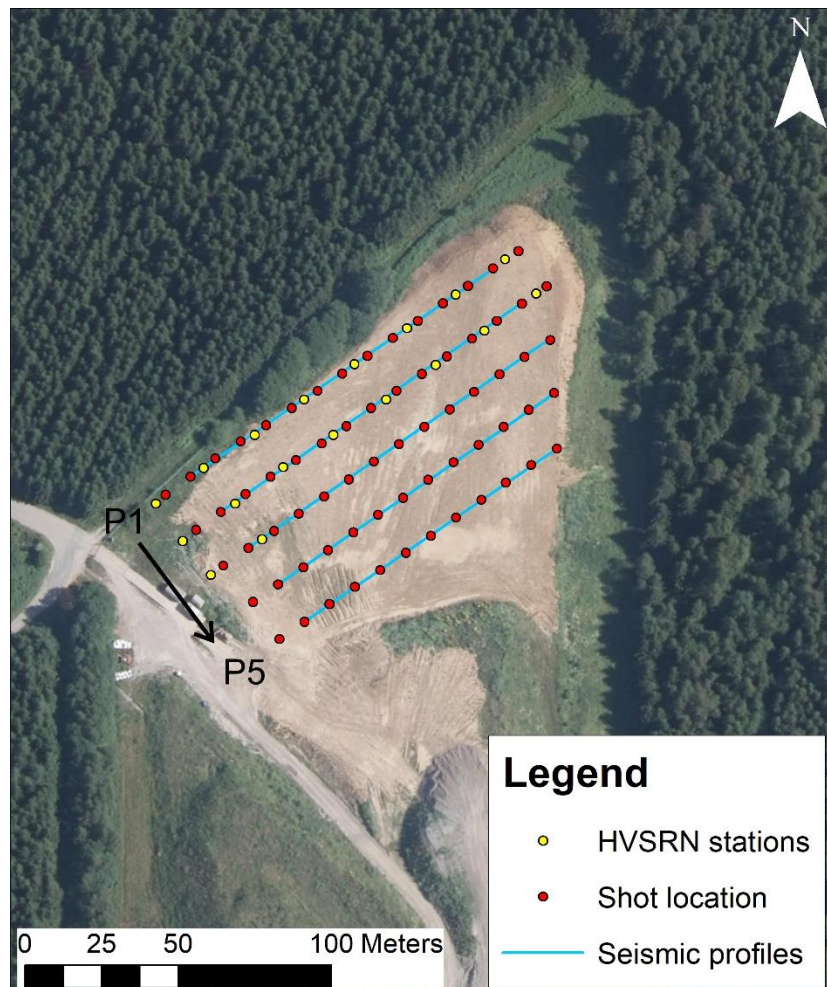


Figure 5: Location of MASW profiles (blue solid lines with red dots as sources) and HVSRRN stations (yellow dots).

Geophysical processing and results

Data processing and results of each geophysical method are described in the following section. A conclusion at the end of the section discusses the overall interpretation with respect to the available historical information.

EM results

The results of the EM measurements are shown as maps in *Figure 75*. These maps display the quadrature (related to the apparent electrical conductivity - A, C, E) and the in-phase (related to the magnetic susceptibility - B, D, F) of the received signal at three different depths below surface corresponding to the depths of maximum sensitivity of the EM antenna configuration.

At a depth of 0.5 m, the contrast of apparent conductivities (*Figure 75 A*) is not high between the landfill and its surrounding. Only the westernmost part of the map shows higher electrical conductivities. These high values are simply due to the truck scale system located near the entrance of the site. In terms of magnetic susceptibility (*Figure 75 B*), although the contrast is also relatively low, a difference can still be observed between the western and eastern parts. It may be due to different materials used for the capping layer. It is to be noted that two linear structures (NW-SE oriented) are detected and seem to divide the landfill into three. These may be drains. Deeper down, a more conductive area appears in the central part of the landfill (*Figure 75 C and E*). This area may possibly correspond to the top of MSW. The fact that the conductive anomaly does not extend over the whole landfill area suggests that the extent of the MSW deposits is limited or that the cover layer is of varying thickness. The contrast of magnetic susceptibility also increases with depth, suggesting a higher metallic content.

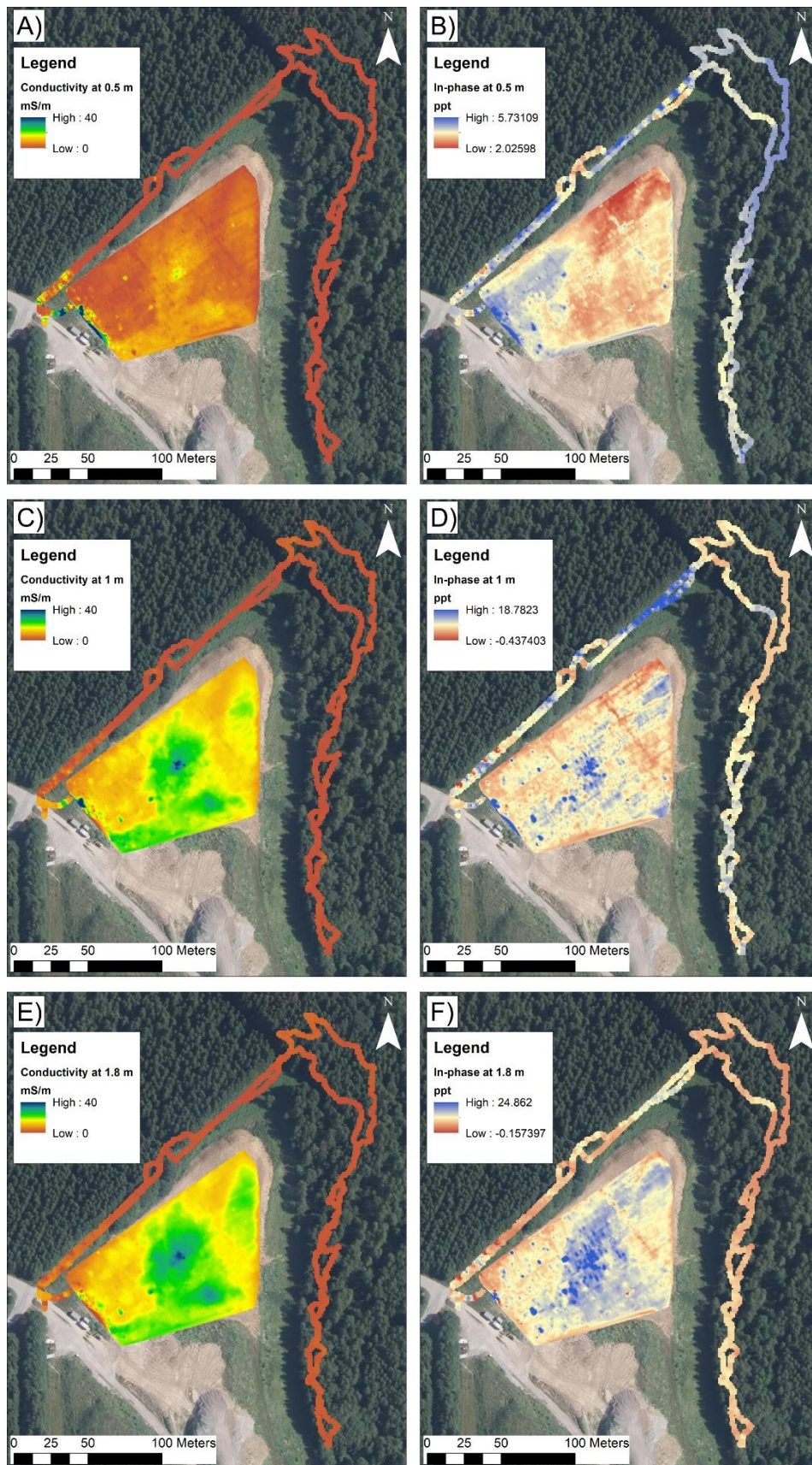


Figure 6: EM results. Electrical conductivity maps at 0.5, 1 and 1.8 m depth (A, C, E). In-phase values (related to magnetic susceptibility at 0.5, 1 and 1.8 m (B, D, F).

ERT and IP results

Data collected were first filtered by removing all measurements characterized by a repetition error on the measured resistance greater than 5%. Then, in order to weight the data in the inversion process, an error model was calculated on the resistance value using the reciprocal data collected during the acquisition (see *Figure 7*). The absolute error is 2.4E-3 Ohm and the relative error 3.3E-3 % confirming the good quality of data acquired.

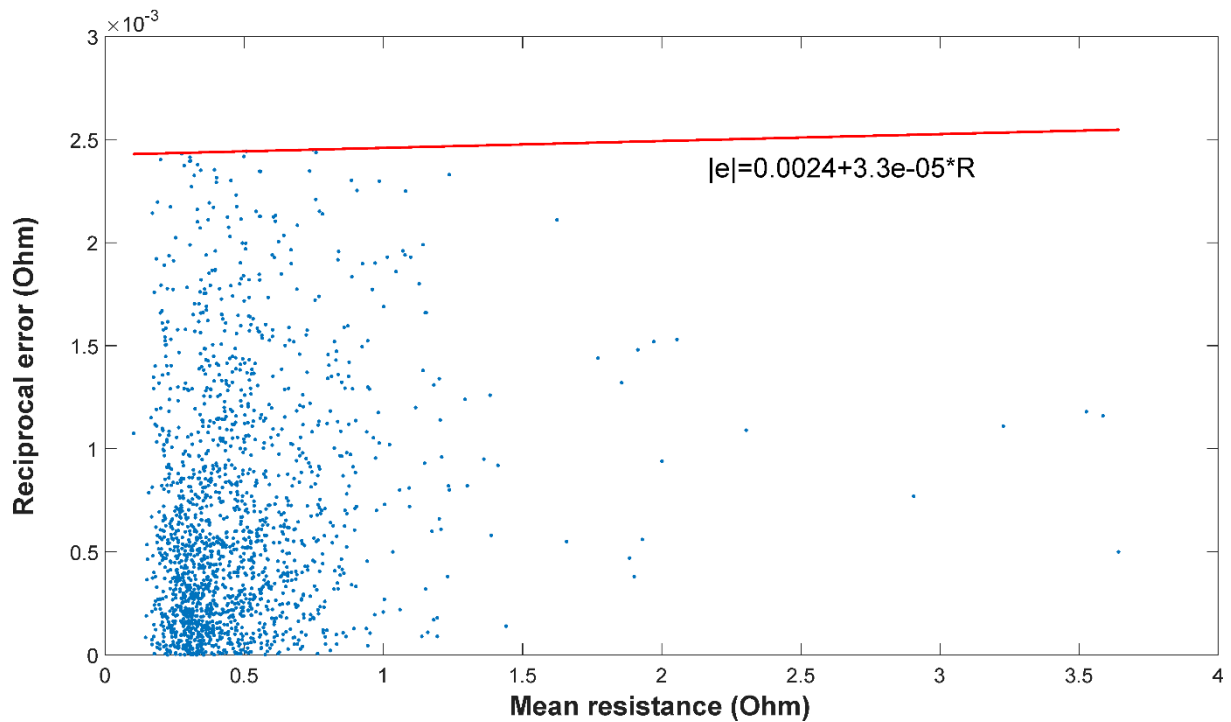


Figure 7: Resistance error model estimated by comparing the normal and reciprocal measurements.

The weighted data were inverted with BERT (Günter *et al.*, 2006) using a robust constraint on the data and a blocky constraint on the model. The 3D models obtained with BERT satisfies the error weighted chi-square, $\chi^2 = 1$ meaning that the data are fitted to their error level. *Figure 77* shows the final 3D resistivity and chargeability models. Note that all coordinates are expressed in Belgian Lambert 1972.

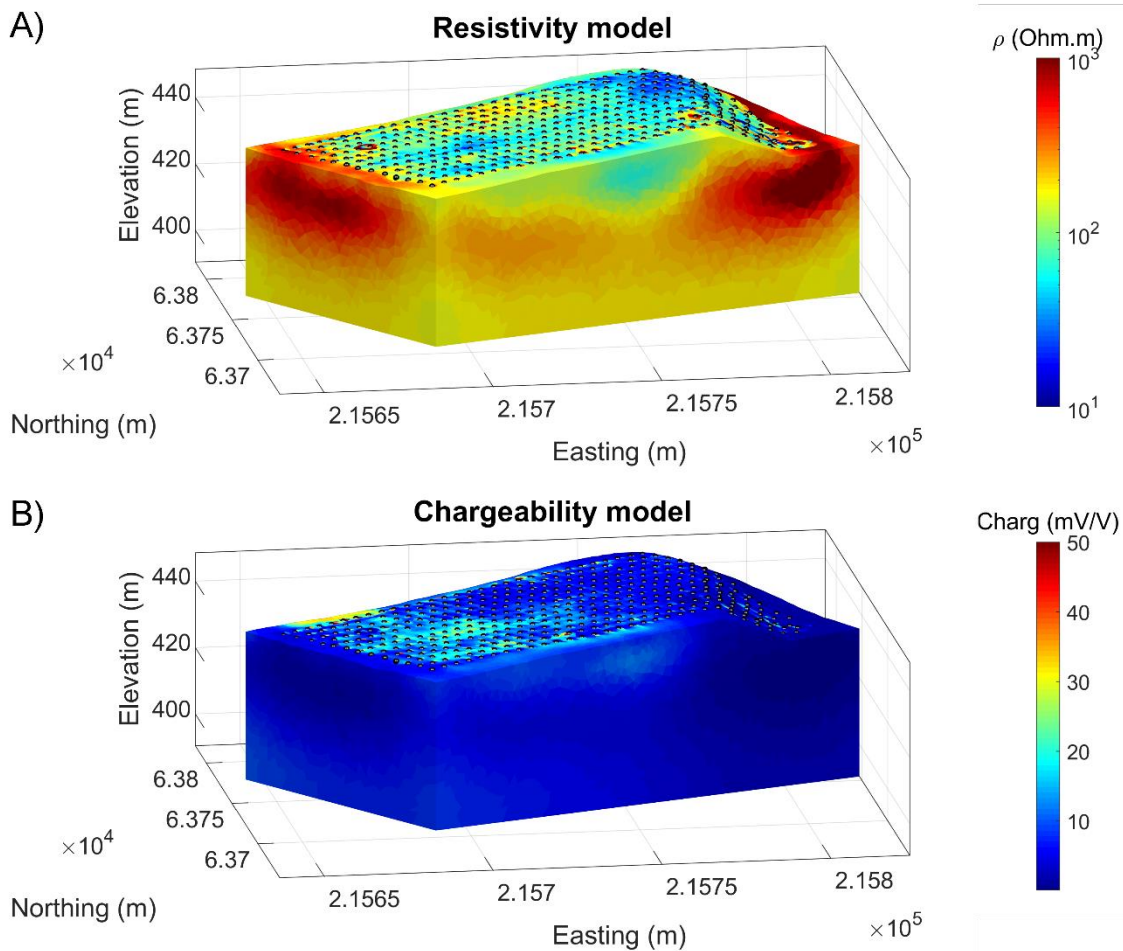


Figure 8: 3D electrical resistivity (A) and chargeability (B) models. The dots on the surface of the models represent the electrodes.

Figure 78 shows a section through the 3D models in the direction of the 7th line of electrodes. The electrical resistivity model (Figure 78A) shows mainly two layers with contrasted signature. The upper layer (which extends to a thickness of about 15 m in the central part of the model) is characterized by low electrical resistivity (<100 Ohm.m) with the lowest resistivity observed at a distance of between 60 and 100 m. This area of low resistivity likely corresponds to the anthropogenic materials (MSW and inert waste) that were deposited in the old quarry. The resistivity of the second layer is higher and is typical of bedrock. In the central part of the model, the resistivity of the “bedrock” layer decreases a bit which could be explained by leachate infiltration or by an effect of the above conductive zone that reduces the model sensitivity. The chargeability section (Figure 78B) also displays two contrasted regions but whose extent differs from the ones of the resistivity models. High chargeability is observed from 10 to 120 m. The highest values are found at around 9 m depth. Such anomalies were also observed at other landfills investigated in RAWFILL which also contained MSW. The difference of extent between the low resistivity (interpreted as “anthropogenic deposits”) and the high chargeability (interpreted as MSW) layers suggests that the landfill contains two types of materials (inert and MSW) which were deposited at different times and not mixed together. At a distance of between 20 to 55 m, a thin layer, more resistive and not chargeable, is observed just above a less resistive and more chargeable one. The lower one has all the characteristics of MSW whereas the upper one is more difficult to interpret given the context but certainly contains less water and less metal (possibly demolition waste/concrete slab?).

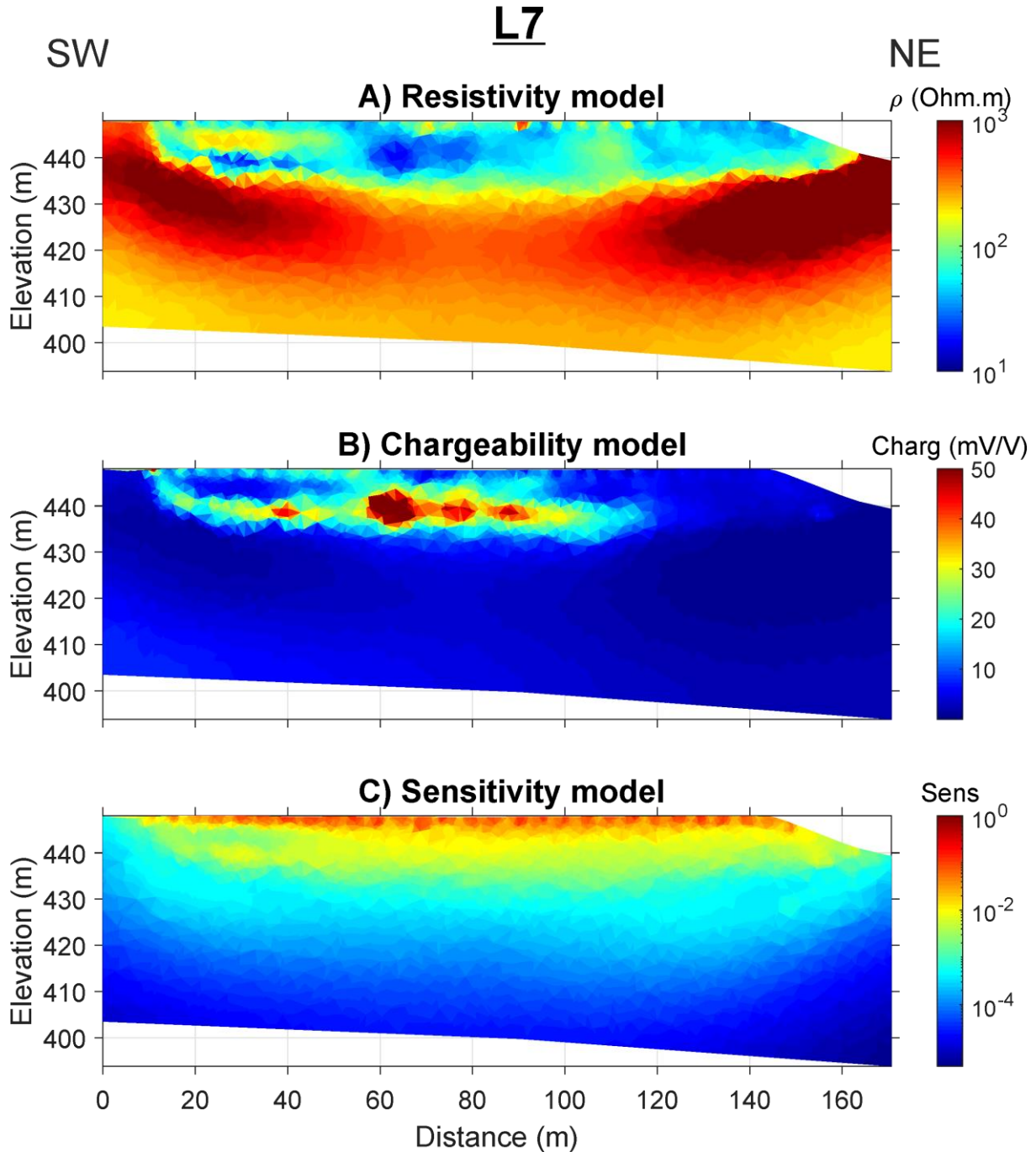


Figure 9: Slice cut through the 3D electrical resistivity (A) and chargeability (B) models along the direction of the 7th line of electrodes. The sensitivity associated to the estimated parameters is displayed in C.

In *Figure 79*, 5 sections (including the one shown in *Figure 78*) are represented. In terms of resistivity, only the leftmost slice (corresponding to the first line of electrodes) has a slightly different structure with a more limited area of low resistivity. Also note the lower resistivity of the “bedrock” in the rightmost slice (corresponding to the 13th line of electrodes) compared to the other slices. This can be explained by a higher water content probably due to greater fracturing of the bedrock and/or a different fluid composition. In terms of chargeability, the highest values are observed in the middle of the model (slice corresponding to the 7th line of electrodes).

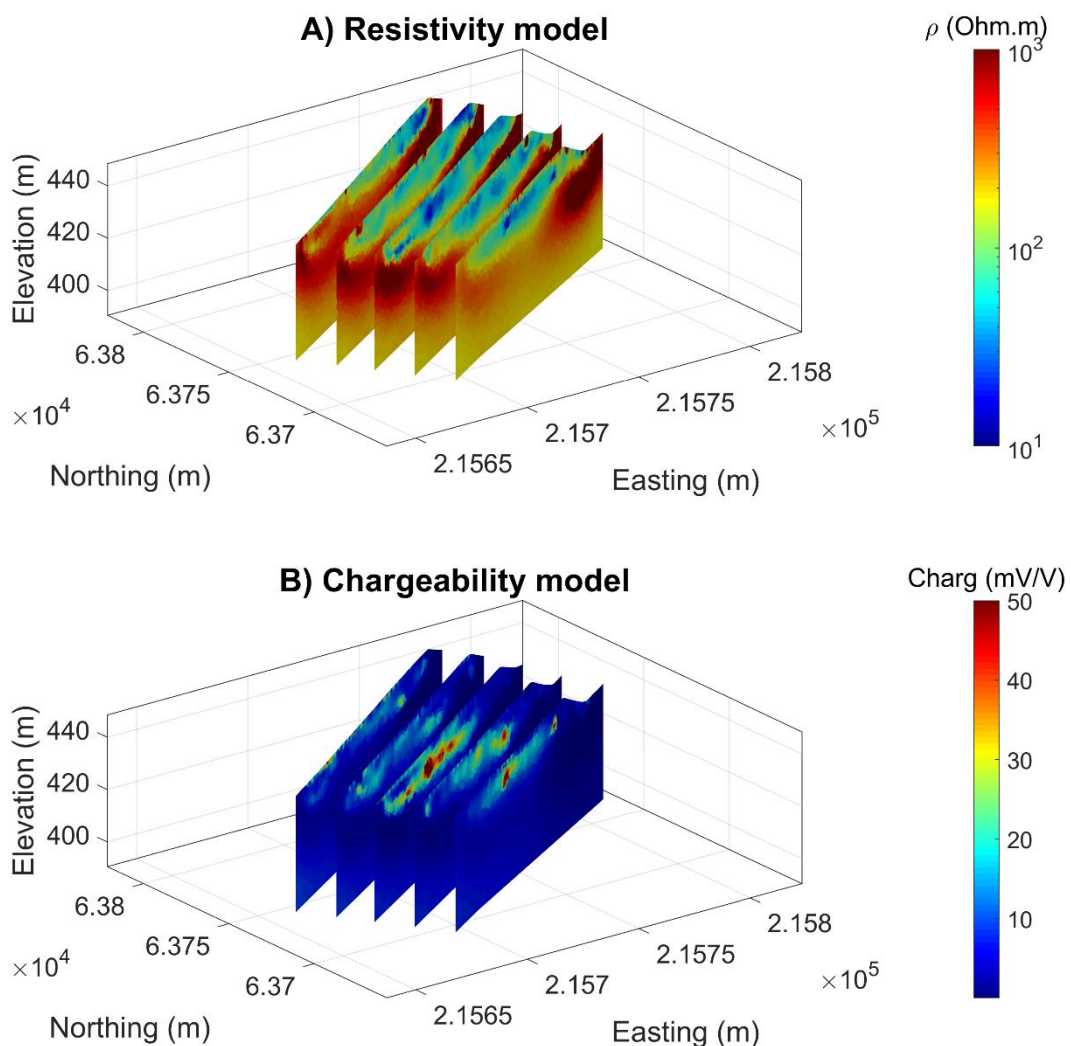


Figure 10: Slices cut through the 3D electrical resistivity (A) and chargeability (B) models along the direction of the 1st, 4th, 7th, 10th and 13th lines of electrodes.

SRT results

The SRT processing (inversion) was carried out with the open source library of pyGIMLi (Rücker et al., 2017). However, only the data from P1 could be inverted. For the rest of profiles, the data were noisy and there was an overlapping between the first arrival of the p-wave and the airwave. Thus, it was not possible to distinguish the refracted p-wave arrivals.

Figure 80 shows the p-wave velocity model of the P1 profile. A shallow layer of low velocity (increasing with depth from 70 to 450 m/s) can be observed and might correspond to the MSW. Below, an intermediate layer of less than 1700 m/s is visible (altered sandstone/shale?). The largest velocity (>2400 m/s) is observed deeper and is within the range expected for sandstone/shale.

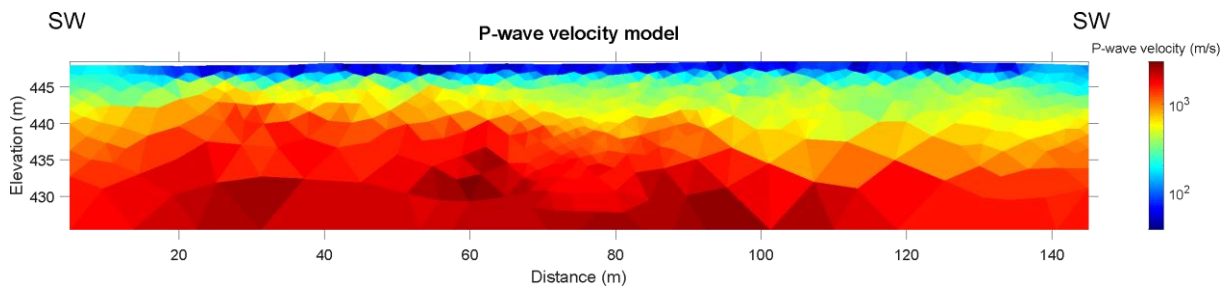


Figure 11: p-wave velocity model obtained along P1.

MASW results

The software SurfSeis6 (Kansas Geological Survey KGS) was used to process the data. As a fixed spread receiver array was deployed, a roll-along data acquisition pattern (i.e. twelve 24-channel records) was first emulated. Each shot record was transformed to calculate the phase velocity-frequency distribution,

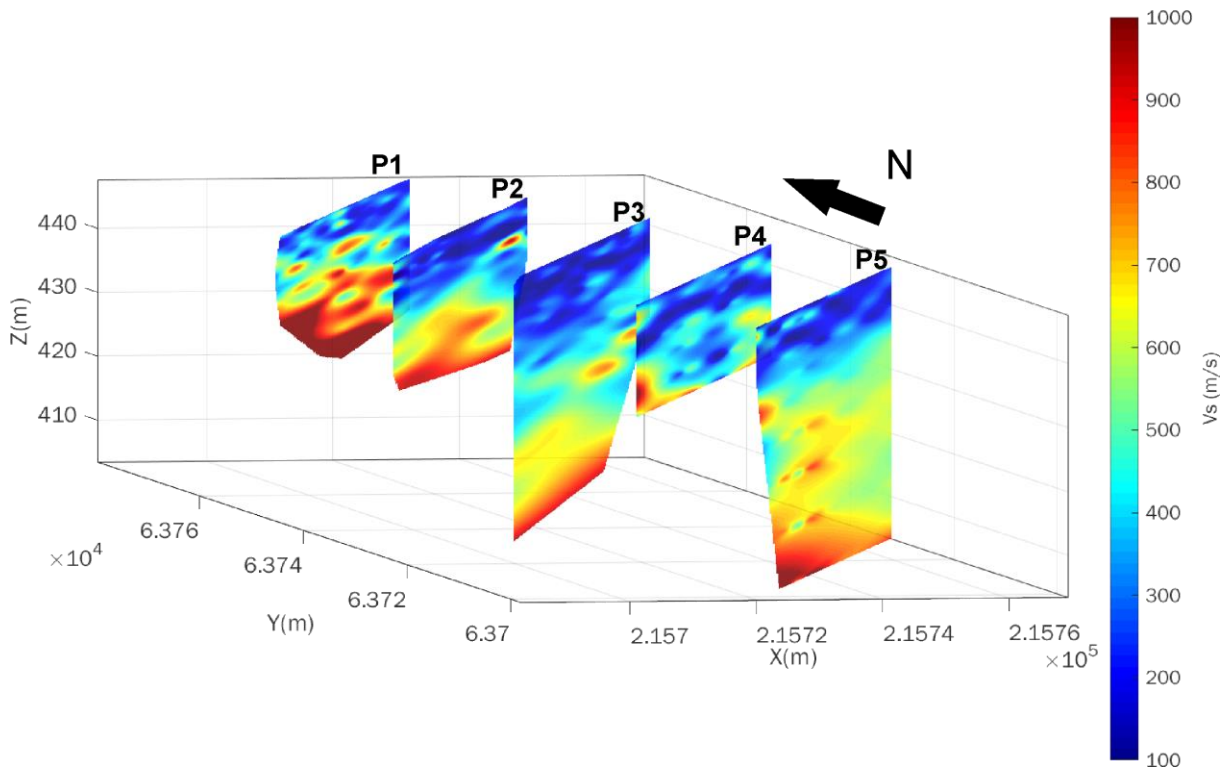


Figure 12: 2D S-wave velocity models obtained from MASW method. Error of the inversion larger than 30% were discarded.

also known as the dispersion curve, and the fundamental mode of each dispersion curve was then picked. Finally, the dispersion curves were inverted from each profile to derive the 2D shear-wave velocity models presented in [Figure 81](#). In general, the picking of the fundamental mode of dispersion curves was very difficult to achieve due to the poor quality of data. This affected the inversion results which show a lot of heterogeneities that can be linked to artefacts. Therefore, the results presented in [Figure 81](#) must be interpreted with caution.

[Figure 81](#) shows a surficial heterogeneous layer of low velocities ranging between 100-300 m/s. The velocity then increases with depth, showing a layer with intermediate velocities of about 600 m/s. The deepest horizon is characterized by velocities higher than 800 m/s. The velocities of the shallowest layer are in agreement with the S-wave velocities of MSW deposits (Carpenter *et al.*, 2013; Dumont *et al.*, 2017; Yin *et al.*, 2017) although some anomalies of higher velocities are also present, especially in P1. The velocities of the deeper layer correspond to the velocities of sandstone/shale (e.g. Kassab and Weller, 2015) which is the host material. The layer with intermediate velocities (400-800 m/s) might correspond to altered and/or more saturated sandstone. In general, sandstone/shale exhibits a wide range of S- and P- wave velocities depending, for example, on their porosity and water-saturation (Wang *et al.*, 2019).

It should be noted that the depth of investigation in P1 is limited compared to the rest of the profiles. The dispersion curves obtained along P1 were highly contaminated with energy from higher order modes at low frequencies, this probably due to a near-field scattering and body waves (Li *et al.*, 2020).

HVSRN results

The open-source software GEOPSY (SESAME European Project) was used for the processing of the HVSRN data. At each station, the ambient vibrations were recorded in three components: a signal in the north-south direction, east-west and vertical directions. Then, for each station the following process was done: 1) selection of N stationary windows in the three components, 2) computation of Fourier spectra for each window, 3) averaging of horizontal components, 4) computation of the spectral ratio between the horizontal and the vertical component, 5) computation of the average HVSRN. The time series were sliced in windows of 25 s and a 60% of overlap, giving between 76 and 100 windows in total (depending on the level of non-stationary noise).

Well-separated peaks in the HVSRN spectrum might be associated with layers characterized by different impedances and/or thicknesses (Piña-Flores *et al.*, 2017). For most of the computed HVSRN spectra in Bertrix, several peaks were observed which highlights the heterogeneity of the site and further complicates the interpretation of data without ground truth calibration values ([Figure 82](#)).

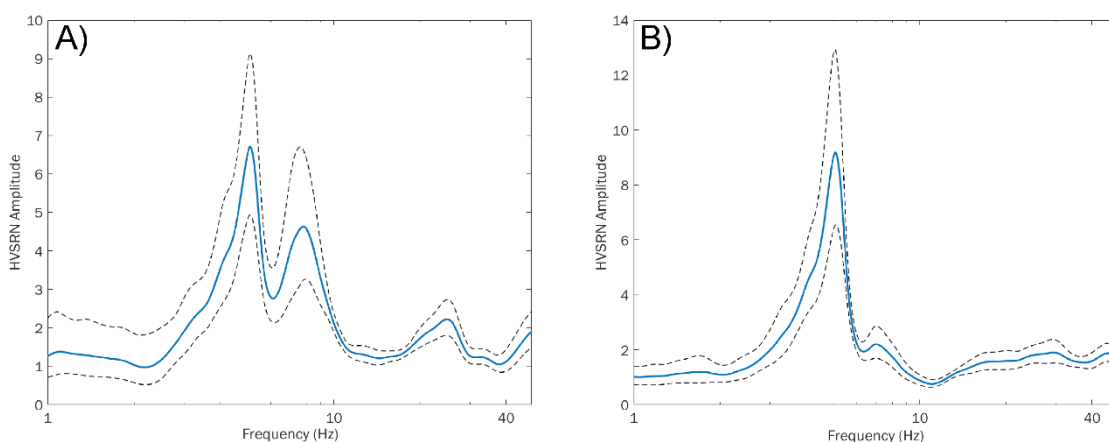


Figure 13: Examples of HVSRN-amplitudes at two stations showing multiple peaks. The solid line is the HVSRN amplitude averaged over all the time windows and the two dashed lines represent the standard deviation. At some stations, the peaks can be clearly distinguished (A) whereas at other stations it is more difficult (B).

To visualize the fundamental peak(s) and its (their) continuity along the seismic profiles P1 and P2, the HVS RN amplitude are shown along the position of all the stations (see *Figure 83*). Only two H/V stations were taken in P3, herein not considered. In P1 and P2, two main peaks are observed between 2 and 10 Hz (see black dots in *Figure 83*). Their amplitude increases towards north-east.

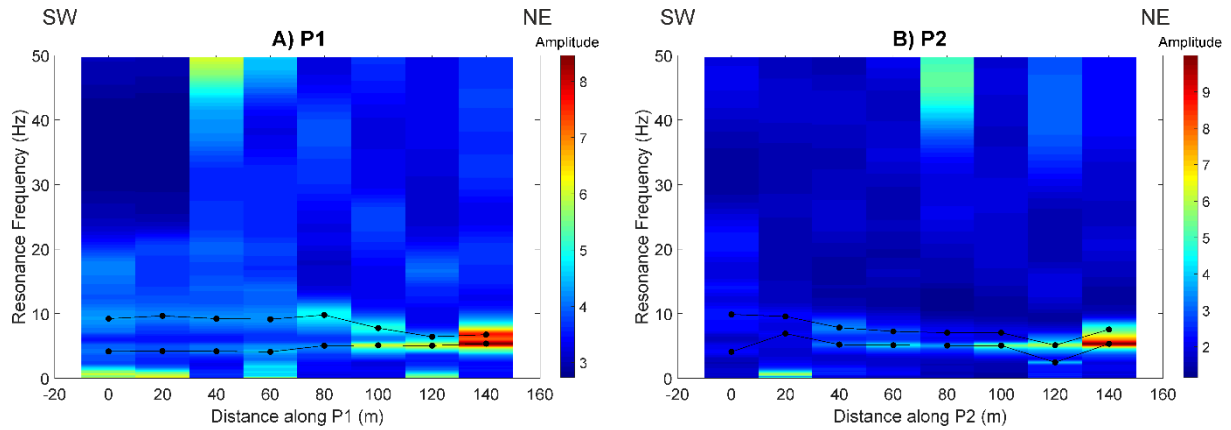


Figure 14: Peak frequencies in function of the position along the profiles (P1 = A, P2 = B). The size of the dots represents the amplitude of the peaks.

The peak frequencies - f_{β_1} and f_{β_2} - were used to roughly determine the thickness h_1 and h_2 along all the HVS RN stations. For this purpose, the shear-wave velocities previously estimated with MASW and the following formulas were used:

$$f_{\beta_1} = \frac{\beta_1}{4h_1} \quad f_{\beta_2} = \frac{1}{4 \left(\frac{h_1}{\beta_1} + \frac{h_2}{\beta_2} \right)}$$

where β_1 and β_2 are the Shear-wave velocities of layers 1 and 2 and $f_{\beta_1} > f_{\beta_2}$. According to the velocities observed from MASW, a shallow layer of velocity $\beta_1 \cong 200$ m/s over a deeper layer of velocity $\beta_2 \cong 600$ m/s can be assumed.

Figure 15 shows the estimated thickness of first layer (solid line) on top of the p-wave velocity model along P1. The location of the HVS RN stations is displayed as black dots. The interface between the first and second layer seems to correspond to the zone where the p-wave velocity increases rapidly and could therefore indicate a transition between anthropogenic material and the host rock. As the estimated base of the second layer goes beyond the extent of the figure, it is not displayed here. The results obtained along the second profile (not displayed) globally show similar trend except at the station located at 120 m where the estimated thickness is much greater and therefore unlikely.

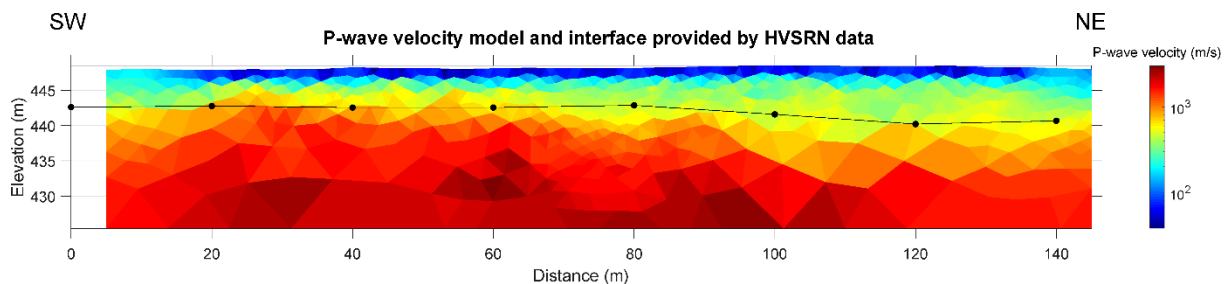


Figure 15: Results of the HVS RN method together with the inverted p-wave model in P1. The black dots represent the HVS RN-stations whereas the solid black line represents the estimated interface between the first and second layer.

Summary of geophysical findings

EM mapping clearly shows areas with different properties likely related to different waste composition. While the seismic results are difficult to interpret (with a few exceptions), it is clear that the most valuable information is provided by ERT and IP methods. They reveal strong lateral and vertical variations which are probably due to different waste composition.

Targeted sampling

In order to validate and calibrate geophysical results, a sampling plan targeting electrical anomalies (*Figure 16*) was proposed to the site manager but has not yet been implemented.

Z= 439 m (9 m depth)

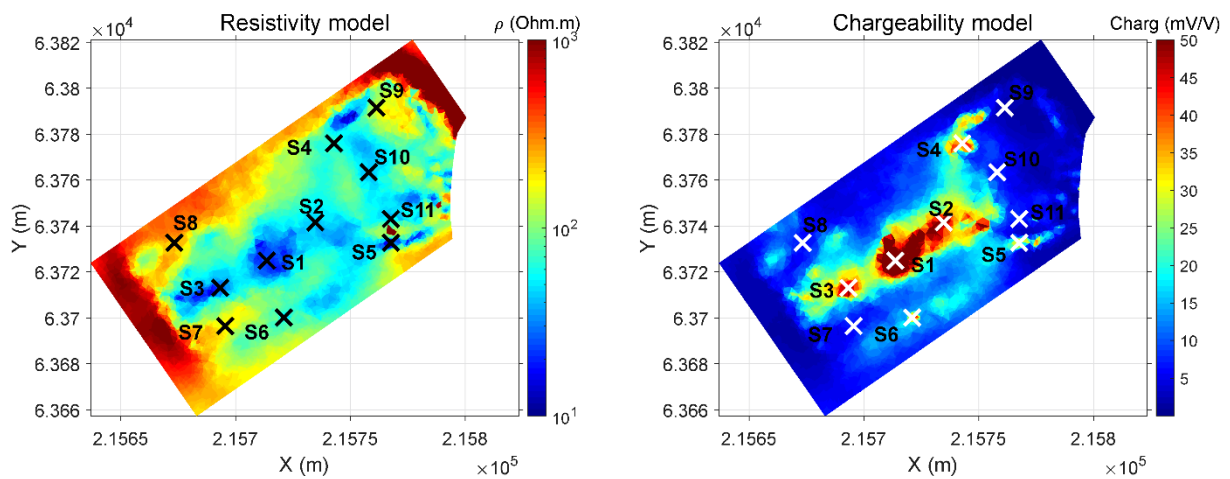


Figure 16: Sampling plan targeting electrical anomalies.

Correlation analysis

Comparison between seismic and electrical models

A comparison between the seismic refraction model obtained in P1 and a section cut through the ERT/IP model at the same location may reveal useful information and strengthen the interpretation (*Figure 86*). Overall, the two types of models show similar features, i.e., the thickness of “anthropogenic” deposits (low resistivity, low p-wave velocity) tends to increase north-eastward. However, the thickness provided by the electrical resistivity (*Figure 86B*) appears to be slightly greater than that provided by the seismic model in the northeast part of the model. Furthermore, the low resistivity anomaly observed at a mean elevation of 440 is invisible in the p-wave velocity model, probably because it is characterized by lower velocity than the above material. However, without ground truth data, it is difficult to further interpret the results.

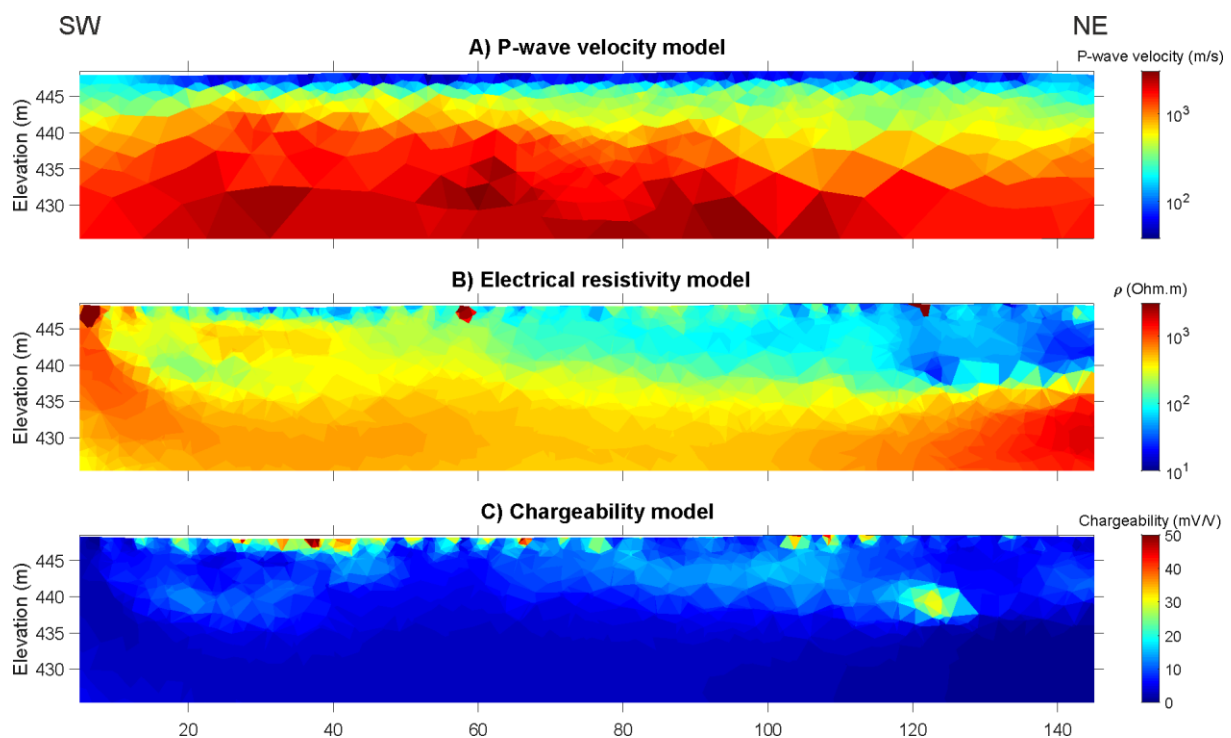


Figure 17: 2D p-wave velocity model of the P1 profile (A), 2D slices of electrical resistivity (B) and chargeability (C) extracted from the 3D models along P1.

Comparison between available historical data and electrical models

Given the low amount of historical data available, only a comparison with remote sensing data is provided. Aerial photographs of the site taken at different times show its recent evolution (see *Figure 87 A and B*). Apart from the evolution of the vegetation cover (due to an addition of topsoil in 2017 over the whole study area), the main changes occur in the north-eastern part of the site which has been filled with inert waste. This is clearer in the hillshade views (*Figure 87 C and D*) obtained from the digital elevation models collected in 2013 and in 2020. They also show that a depression to the south of the study area has in the meantime been filled in the meantime. Unfortunately, no aerial photograph has been collected during the period when the site was filled with MSW.

The previous comparison helps to identify zones that have been recently backfilled with inert material.

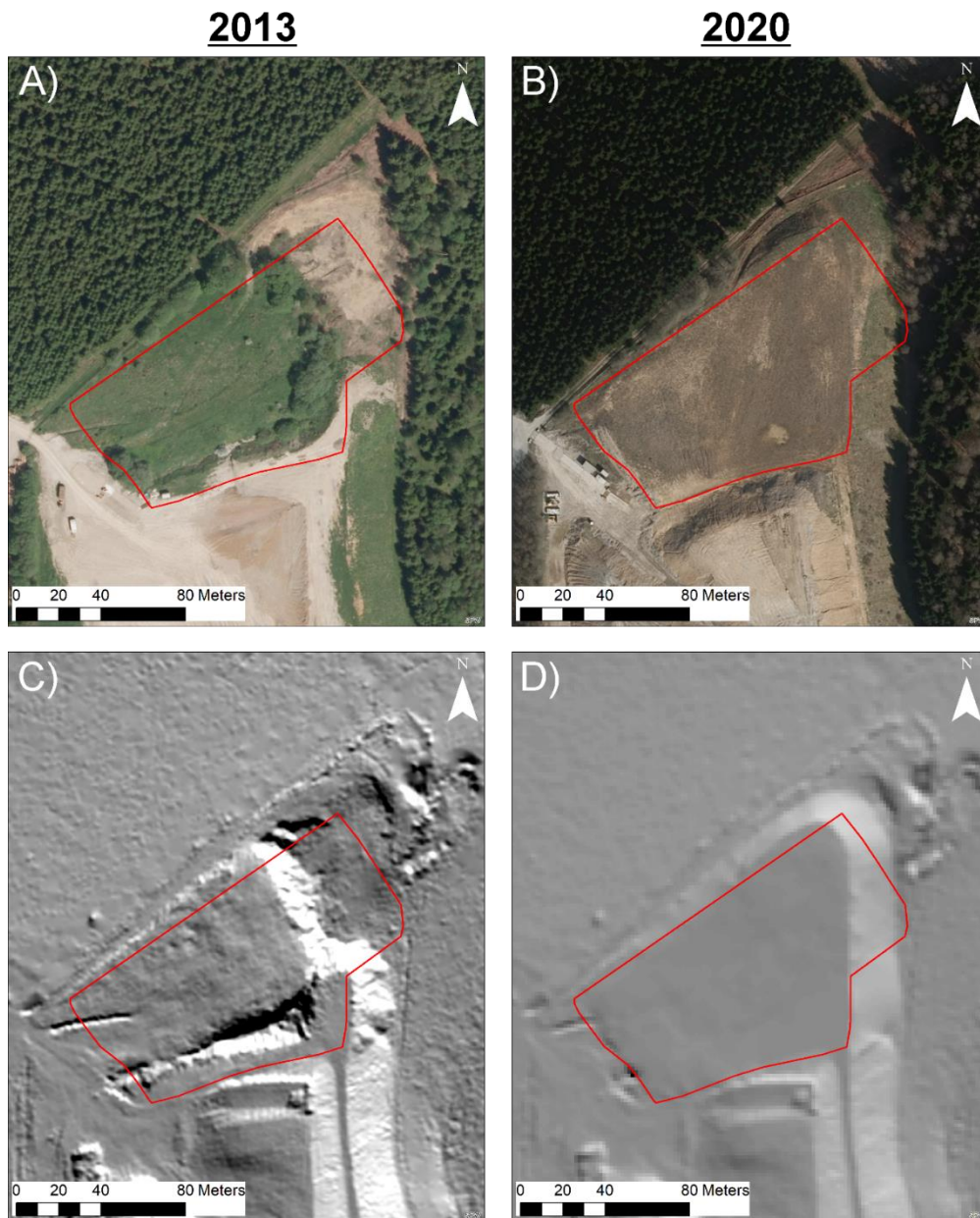
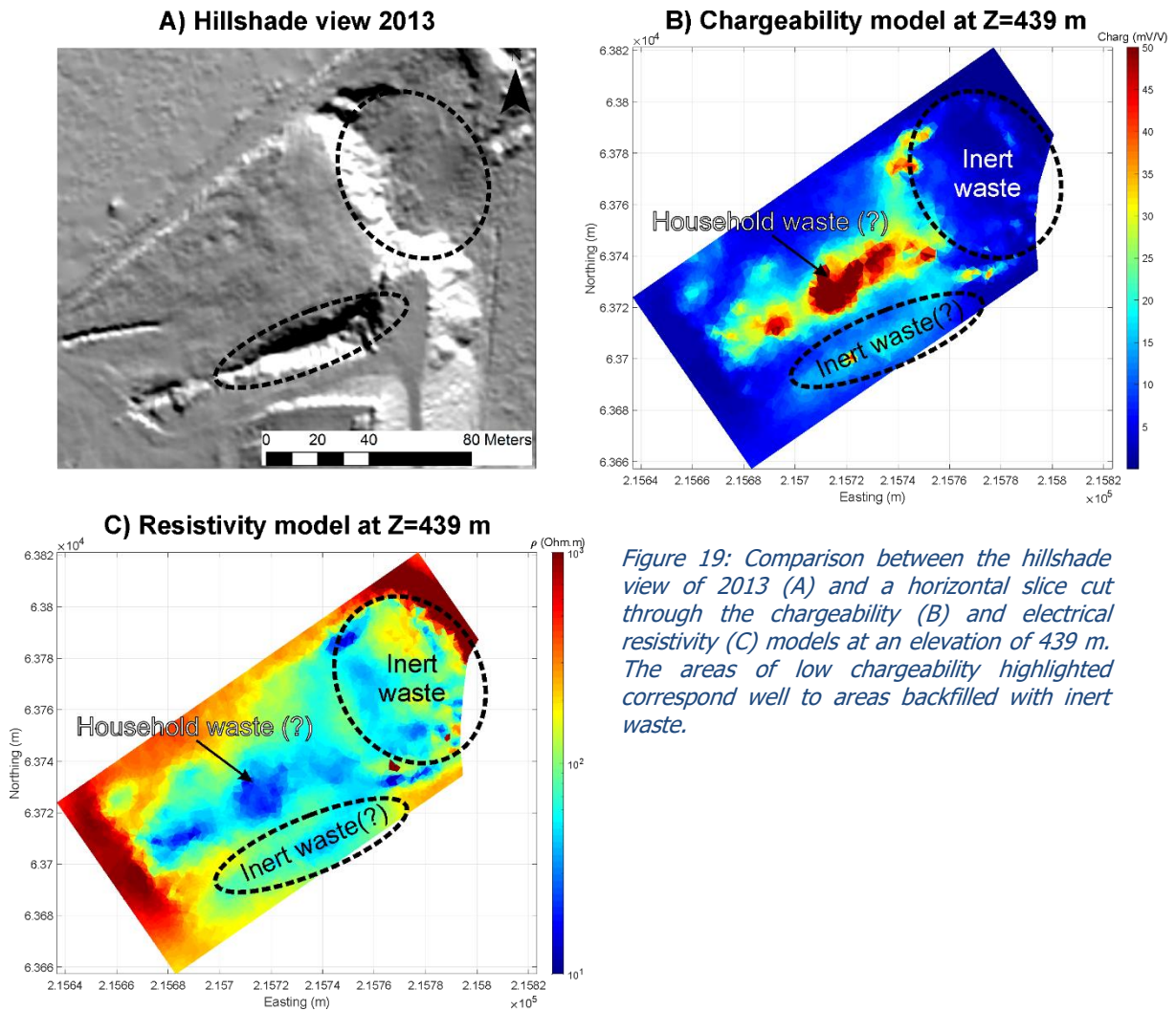


Figure 18: Aerial views of the Bertrix landfill taken in 2014 (A) and in 2018 (B) together with a hillshade view of the site based on the digital elevation model taken in 2013 (C) and in 2020 (D).

Looking at a horizontal slice cut through the chargeability and resistivity models at an altitude of 439 m (see *Figure 88*), it is evident that the backfill material in the north-east is characterized by low chargeability. At the location of the southern depression, the chargeability is somewhat higher, suggesting a slightly different composition of backfilling material. In terms of resistivity, the recent deposits are characterized by low to medium values, with greater heterogeneity in the north-eastern zone.



Resource Distribution Model

Given the absence of any ground truth data, the construction of the RDM is based solely on geophysical data, which is not ideal. However, the relatively large contrast of properties obtained allows the use of a clustering algorithm to partition the domain into clusters. In this case, the k-means clustering algorithm was chosen. The spatial coverage of the seismic properties being limited, the classification was only performed with the electrical properties.

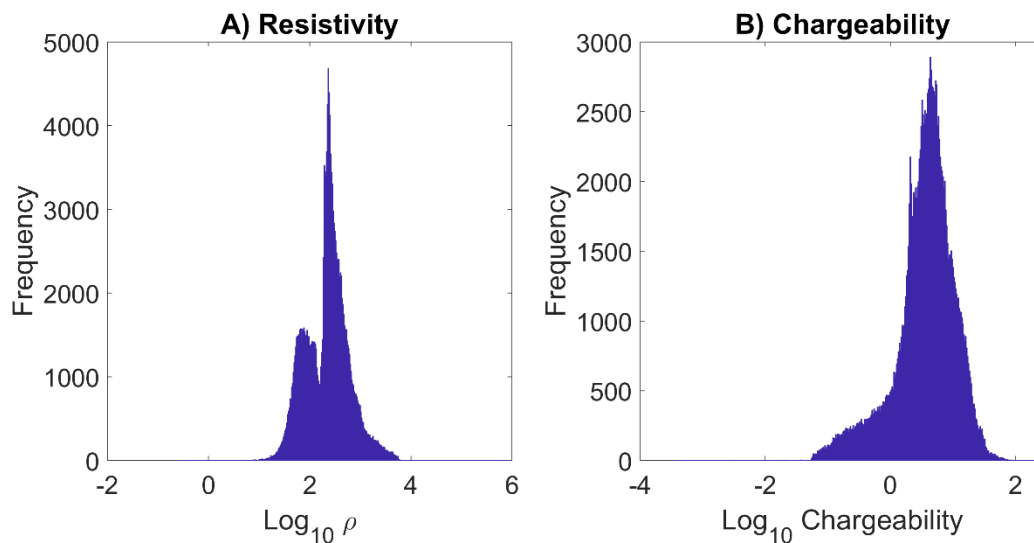
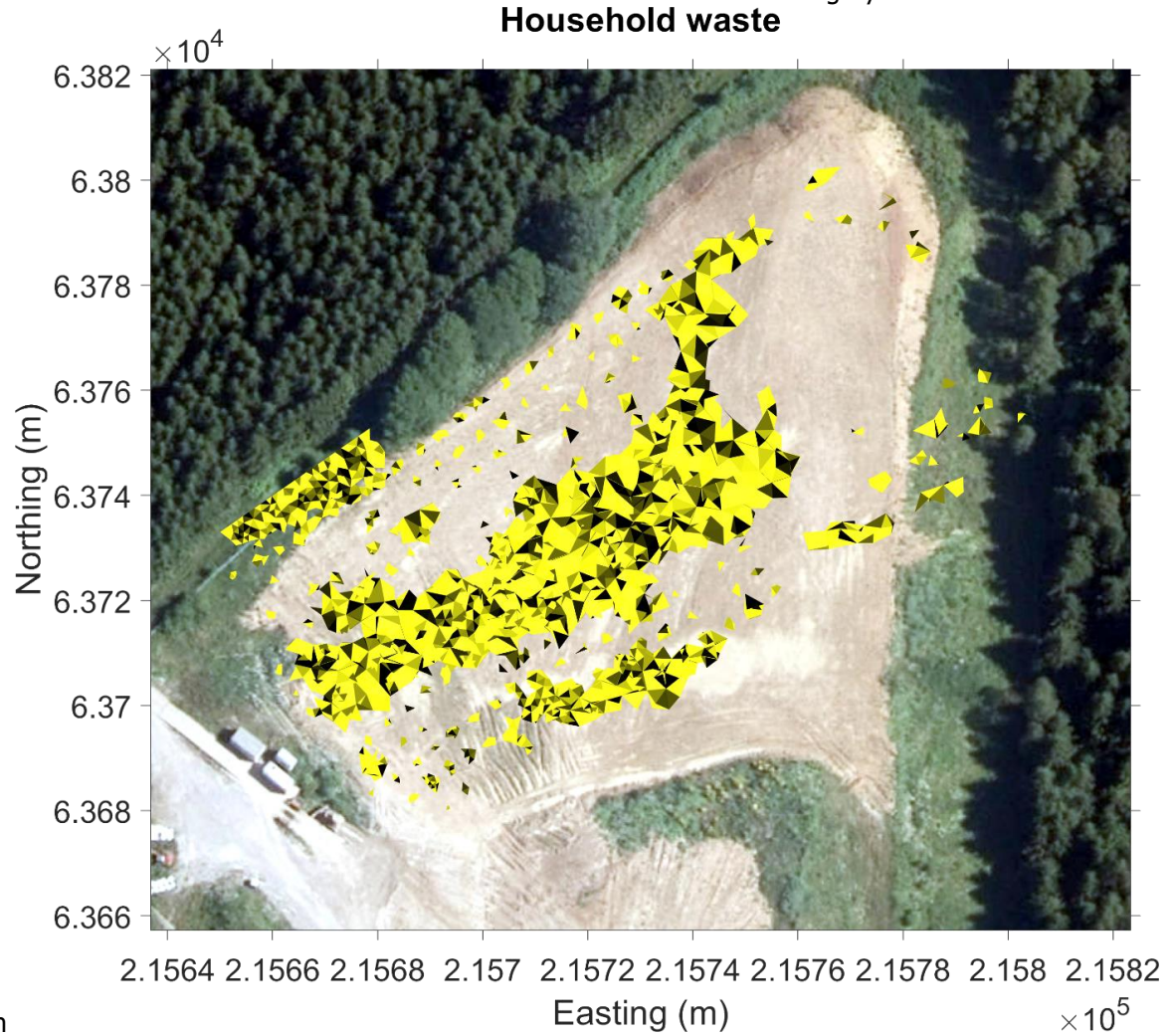


Figure 20: histograms of electrical resistivity and chargeability

The clustering process was a two-step process. First, it was carried out with the resistivity model by considering two clusters because resistivity mainly shows two populations (see [Figure 89](#)). The hypothesis followed is that the low resistivity corresponds to anthropogenic materials (it can however also include the host material affected by leachate infiltration). The corresponding volume is 127 500 m³. A representation of the latter is provided in [Figure 21](#).

In a second step, the same algorithm was applied on the chargeability data. Here the high chargeability data were attributed to MSW. The volume calculated for the latter category is 15 500 m³. It is shown



in
Figure 22.

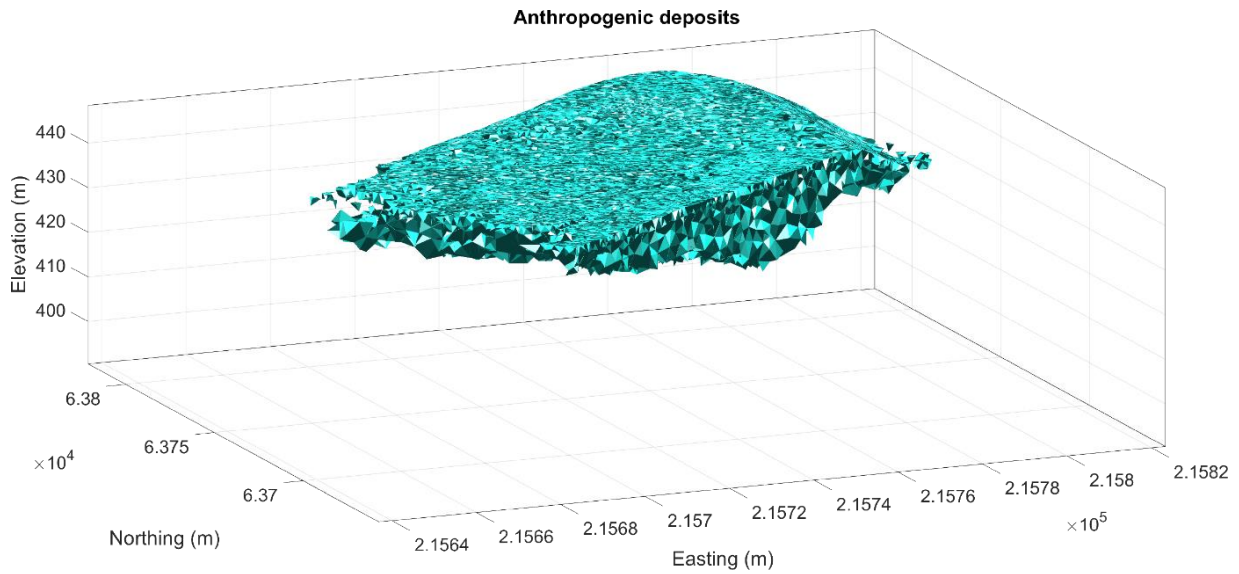


Figure 21: 3D representation of the anthropogenic material (household waste, inert waste) estimated after the clustering with a K-means algorithm. The total volume is 127 500 m³. The latter number can also include the natural soil below the landfill that was potentially impacted by leachate infiltration.

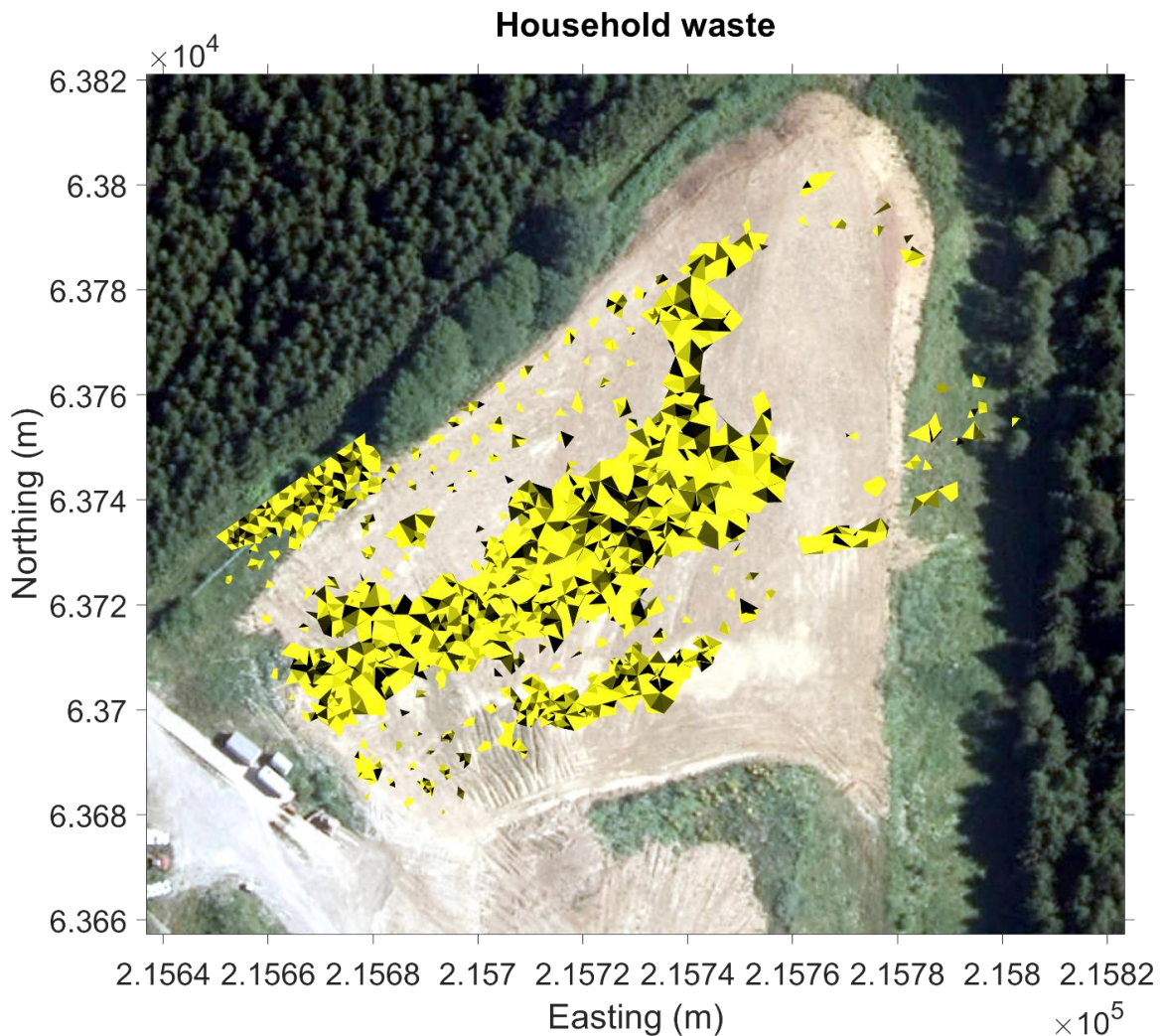


Figure 22: 3D representation of the MSW obtained with the K-means algorithm. The estimated volume is 15 500 m³.

Conclusion

The absence of abundant vegetation or HDPE geomembrane, the fact that the surface was globally flat and the expected high contrast between the physical properties of the waste and the host rock make the Bertrix site, in theory, very suitable for geophysical investigations. Among the methods tested, the electrical ones gave the best results. Although promising, the seismic methods proved to be relatively difficult to interpret notably because of the low velocity of body waves in the waste material (which had an impact on the SRT results), but also because of the presence of noise due to activities on site (truck passage and generator). Given the presence of a cover layer, the results obtained with the EM device were relatively uninformative. Other antennas with a larger penetration depth could have yielded more useful information regarding waste composition and zonation.

Despite these limitations, ERT and IP methods provided useful results due to the high contrast in electrical resistivity between the anthropogenic materials and the host rock on the one hand, and the contrast in chargeability between the waste materials on the other. The results obtained made it possible to construct a RDM which nevertheless suffers from a lack of ground truth data for calibration and validation.

References

Dahlin, T. and Zhou, B. (2006) Multiple-gradient array measurements for multichannel 2D resistivity imaging. *Near Surface Geophysics* 4(2), 113-123.

Dumont, G., Robert, T., Marck, N. and Nguyen, F., 2017. Assessment of multiple geophysical techniques for the characterization of municipal waste deposit sites. *Journal of Applied Geophysics*, 145: 74-83.

Günther, T., Rücker, C. and Spitzer, K. (2006) Three-dimensional modelling and inversion of DC resistivity data incorporating topography—II. Inversion. *Geophysical Journal International* 166(2), 506-517.

Piña-Flores, J., Pertou, M., García-Jerez, A., Carmona, E., Luzón, F., Molina-Villegas, J.C. and Sánchez-Sesma, F.J. (2016) The inversion of spectral ratio H/V in a layered system using the diffuse field assumption (DFA). *Geophysical Journal International*, ggw416.

Contact

Feel free to contact us.

Coordination office:

BELGIUM	SPAQuE Boulevard M. Destenay 13 4000 Liège	c.neculau@spaque.be
----------------	--	---------------------

Contact details of the project partners:

BELGIUM	Atrasol Cleantech Flanders / VITO OVAM Université de Liège	renaud.derijdt@atrasol.eu alain.ducheyne@vito.be ewille@ovam.be f.nguyen@ulg.ac.be
FRANCE	SAS Les Champs Jouault	champsjouault@gmail.com
GERMANY	BAV	pbv@bavmail.de
THE UK	NERC	jecha@bgs.ac.uk

